

# Optical trapping and light-induced agglomeration of gold nanoparticle aggregates

Yi Zhang and Claire Gu\*

*Department of Electrical Engineering, University of California, Santa Cruz, California 95064, USA*

Adam M. Schwartzberg, Shaowei Chen, and Jin Z. Zhang<sup>†</sup>

*Department of Chemistry and Biochemistry, University of California, Santa Cruz, California 95064, USA*

(Received 6 September 2005; revised manuscript received 28 February 2006; published 6 April 2006)

This paper demonstrates the optical trapping of micron-sized gold nanoparticle aggregates (GNAs) with a TEM<sub>00</sub> mode laser at 532 nm and reports the observation of an unusual light-induced agglomeration phenomenon that occurs besides the trapping of the GNAs. The observed agglomerate has a 60–100 μm donut-shaped metal microstructure with the rate of formation dependent on the laser power used. Citrate capped gold nanoparticles also show light-induced agglomeration, yielding different sized microstructures from those produced with GNAs. While the observed trapping can be explained by a model including the optical radiation and radiometric forces, the light-induced agglomeration cannot be explained by these two forces alone as the size of the agglomerate is much greater than the waist of the Gaussian beam used in the optical trapping. We attribute the additional cause of the light-induced agglomeration to ion detachment from the surface of the nanoparticles (aggregates) due to light illumination or heating. This is supported by the observation of reversible electrical conductivity changes of the solution of the nanoparticles (aggregates) upon laser illumination or direct heating. Light-induced agglomeration can be useful in the design and fabrication of microstructures from nanomaterials for various device applications.

DOI: [10.1103/PhysRevB.73.165405](https://doi.org/10.1103/PhysRevB.73.165405)

PACS number(s): 61.46.–w, 36.40.–c, 81.07.–b

## I. INTRODUCTION

Metal nanoparticles have attracted significant attention recently due to their unique optical,<sup>1–4</sup> chemical,<sup>5,6</sup> and other physical properties.<sup>7–9</sup> Gold and silver particles are of particular interest due to their potential applications in various areas including surface enhanced Raman scattering (SERS).<sup>10–15</sup> SERS possesses the molecular specificity of Raman scattering, while magnifying the nominally weak signal by as much as ten orders of magnitude due to the greatly enhanced electromagnetic field at the surface of the nanoparticles upon resonant excitation.<sup>16–19</sup> It has been found that the majority of the enhancement takes place at the junction of aggregated particles<sup>20–23</sup> bringing to light the importance of interparticle interaction, in particular, under photoirradiation.

Recently, we have shown that surface chemistry is an important factor in nanoparticle aggregation that affects the physical properties of the aggregates.<sup>5,6</sup> Stable nanoparticle solution requires a repulsive surface capping layer of ions or molecules. If the capping layer is interrupted, nanoparticles will agglomerate to form aggregates. This can be induced experimentally in several ways. The most common aggregation method for SERS studies is the addition of sodium chloride or pyridine to silver or gold nanoparticles stabilized by negatively charged citrate ions. Sodium chloride induces aggregation by screening surface charges, while neutral pyridine displaces the charged citrate and decreases particle-particle repulsion. Aggregation or agglomeration is a dynamic process that depends sensitively on many factors such as light, heat, embedding environment, and, most importantly, the chemical nature of the surface capping ions or molecules. However, the interplay among these factors and their effects on the agglomeration of nanoparticles has not yet been fully explored.

Optical trapping<sup>24,25</sup> is a promising technique for probing the fundamental properties of metal nanoparticles (aggregates) and for enhancing SERS detection in chemical and biochemical analysis.<sup>26</sup> Optical trapping of nanometer-sized Rayleigh ( $\phi \ll \lambda$ , where  $\phi$  is the size of the particle and  $\lambda$  is the wavelength of the trapping light) metal particles<sup>27,28</sup> has been achieved in three dimensions using TEM<sub>00</sub> beams. However, micron-sized metal Mie particles<sup>29,30</sup> ( $\phi \gg \lambda$ ) can only be trapped in two dimensions with the light focused below the center of the particle (Fig. 1) with TEM<sub>00</sub> beams. Three-dimensional trapping of Mie metal particles has been achieved in a TEM<sub>01</sub>-mode trapping beam or an obstructed laser beam, where the ring-shaped intensity profile increases the axial trapping efficiency.<sup>31–33</sup>

Optical trapping force has been analyzed in detail in conjunction with the applications of optical tweezers. When a particle is near the focus of a Gaussian beam, it experiences a repulsive scattering force and an attractive gradient force simultaneously.<sup>24</sup> When the two forces balance each other out, the particle will be trapped. Two theoretical models have been developed to evaluate the trapping force, based on ray optics<sup>24,31</sup> and electromagnetic wave theory,<sup>33–35</sup> respectively. Both models agree with experimental measurements of dielectric Rayleigh and Mie particles. In the case of trapping micron-sized metal particles, both models could be used but ray optics is more suitable for analyzing the radiation force due to the large particle size.

In addition, when optical tweezers are used to trap particles, heat can be generated due to light absorption. As a result, the particles can be heated to high temperatures, especially at the laser focus and when the nanoparticles have strong absorption at the laser wavelength. In this case, aberration-radiometric force, generated by the heat flow at the focus due to nonuniform heating of the nanoparticles,

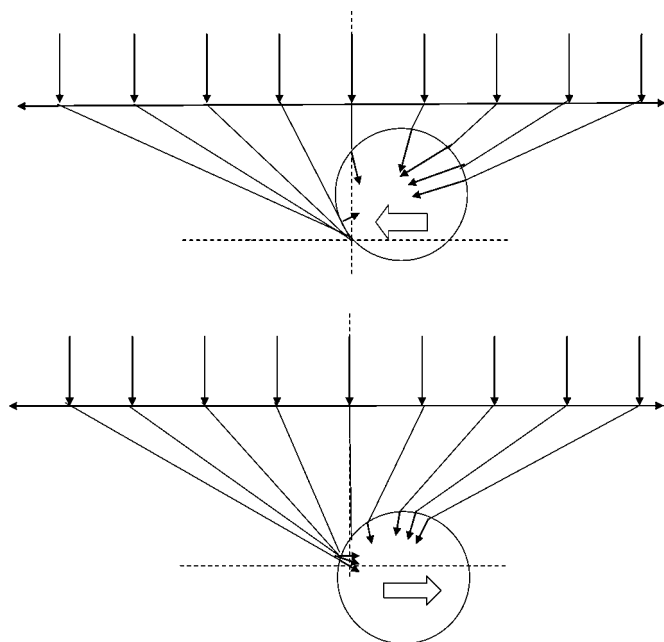


FIG. 1. Two different configurations of light focused on a spherical metal particle. (a) The focal plane is below the center of the metal particles and a net attractive force is generated to pull the particle to the focus. (b) The focal plane is above the center of the metal particle and a repulsive force is generated to push the particle out of the focus (adapted from Ref. 30).

becomes important and needs to be taken into consideration.

Trapping of large metal nanoparticle aggregates has been challenging due to the irregular shapes of the aggregates. In this study, we have found that only a small number of aggregates can be trapped in a stable manner. While regularly shaped particles such as spherical or elliptical particles could be readily trapped, most irregularly shaped aggregates were repelled or spun around at the focus of the laser beam.

Interestingly, in the process of observing the trapping of gold nanoparticle aggregates (GNAs), we have found that light can induce further agglomeration of the aggregates. While optical trapping can be explained by a model based on the radiation and radiometric (thermal) forces,<sup>36–38</sup> the light-induced agglomeration indicates an additional mechanism in operation. We attribute the additional cause for the observed agglomeration to an optical or thermal detachment of ions from the nanoparticles (aggregate) surface. This suggestion is supported by an independent study of reversible changes of the electrical conductivity of the nanoparticles (aggregate) solution upon laser illumination or direct heating.

## II. EXPERIMENTAL METHODS

### A. Nanoparticle synthesis

GNAs were synthesized by the method of Schwartzberg *et al.*<sup>5</sup> Briefly, 500  $\mu\text{l}$  of a 0.02 M  $\text{HAuCl}_4$  stock solution was diluted to  $5 \times 10^{-4}$  M with Milli-Q water in glassware cleaned in aquaregia and rinsed with Milli-Q water to avoid contamination. To this, 40–60  $\mu\text{l}$  of a 0.1 M solution of  $\text{Na}_2\text{S}$  aged 2–3 months was added. After approximately

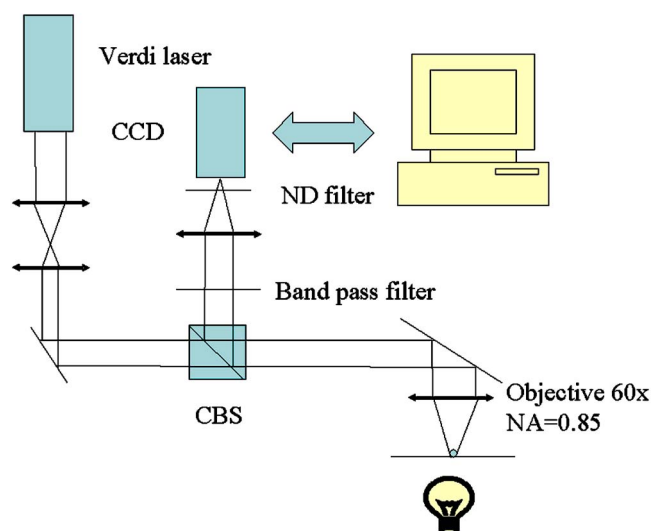


FIG. 2. (Color online) Schematic of experimental setup for the optical trapping and light-induced agglomeration studies.

60–120 minutes, the color changed from a straw yellow to deep purple with the extended plasmon band (EPB) growing in between 600–1000 nm, indicating reaction completion. The aggregate formation is signified by a strong near infrared (NIR) absorption band at wavelengths longer than 600 nm. This synthesis yields gold aggregates capped with sulfur-oxygen species, the nature of which is not entirely known. However, it is believed that these species not only stabilize the particles, but also induce stable aggregation.

Gold nanoparticles of approximately 40 nm were synthesized by the Turkevich method,<sup>39</sup> and silver nanoparticles were synthesized by the Lee method.<sup>40</sup> These procedures involve the reduction of metal salts by sodium citrate in a boiling aqueous solution resulting in citrate capped nanoparticles.

### B. UV-visible spectroscopy, TEM, and AFM measurements

Transmission electron microscopy (TEM) measurements were carried out with a JEOL transmission electron microscope (Model JEM-1200EX). The samples were prepared by drying one drop of the GNAs solution on a sample holder. The measurements were run at 80 KV with a Gatan Bioscan Model 792 camera. A Veeco Bioscope 2 atomic force microscope (AFM) was used to take the three-dimensional (3D) pictures of a single GNA. The sample was scanned using a commercially available piezoelectric scanner (Physik Instrument) and control electronics (Digital Instruments). To further test the property of the GNAs, optical absorption measurements were performed on an HP 89532A spectrometer with 2 nm resolution.

### C. Optical trapping and light-induced agglomeration

Figure 2 shows a schematic of the optical trapping instrumentation. A cw Verdi laser at 532 nm with a maximum laser power of 2 W was used in the experiment as the trapping light source. The diameter of the laser beam was reduced

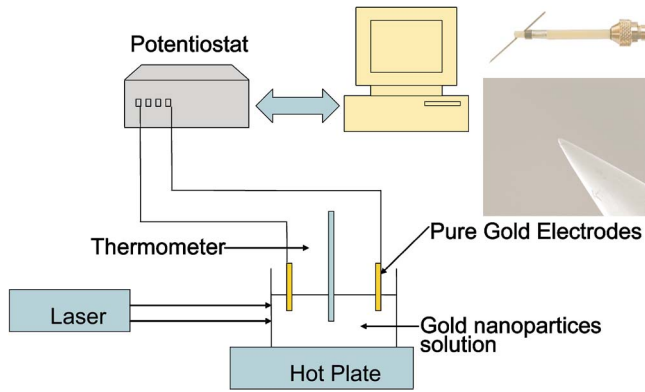


FIG. 3. (Color online) Experimental setup for the electrical conductivity measurement. The change of conductivity is induced by either laser illumination or hot plate heating. The temperature is recorded for both cases to make sure that the temperature changes are the same. The inset shows the scanning electron microscopy (SEM) picture of the tip of gold electrode and how it is assembled with the holder. This type of probe is used for the electrical conductivity measurement.

before entering the  $60\times$  objective lens (numerical aperture = 0.85), however, the effective numerical aperture (NA) was 0.64 because the objective lens was pointed into the water solution (with GNAs). The trapping and agglomeration were observed with a charge coupled device (CCD) camera mounted behind a cubic beam splitter. Another lens ( $f = 10$  cm) was placed in front of the camera in order to observe the image at the focus of the objective lens. The lamp on the right bottom was used for imaging. The green light (532 nm) was filtered out by a bandpass filter.

#### D. Electrical conductivity measurement

Figure 3 shows the experimental setup of the electrical conductivity measurements. The electrical conductivity of a solution of GNAs was measured under various conditions with a computer-controlled potentiostat (SI-1280B). Two gold electrodes were inserted into the GNA solution with a spacing of 2 cm and an external 3 V potential was applied. The electrodes were about 2 cm long and the diameter was about 1 mm with a tip diameter of  $50\ \mu\text{m}$  (Fig. 3 inset). About 75% of the entire electrode was immersed into the solution. A thermometer was also inserted into the solution between the electrodes to trace the temperature change of the solution.

At first, the sample was illuminated with another cw Verdi laser with an output power 3 W at 532 nm between the electrodes with constant stirring to ensure thermal consistency throughout the solution. Afterward, the solution was cooled down back to its original temperature. Next, the solution was heated with a hot plate without laser light. The current change was recorded as a function of time in the cases of both laser illumination and direct heating.

### III. SIMULATION METHOD

Accurate modeling of the radiation force exerted on nanoparticle aggregates requires the knowledge and consideration

of the size, shape, and arrangement of the constituent nanoparticles. Such an analysis would allow us to examine the details of forces acting upon every point on the surface of an aggregate. However, as we are mostly interested in the overall force experienced by an aggregate whose detailed feature size is on the order of a few nanometers (5–10 nm as in Fig. 5 and related discussions), which is much smaller than the wavelength of light used in our experiments (532 nm), we treat each aggregate as a metal particle with an effective complex refractive index. In our experiments, we also observed various irregular shapes of the aggregates. To simplify our analysis, we analyze the forces exerted on a spherical metal particle. These approximations allow us to obtain an estimate of the radiation force.

The mechanism of trapping a metal particle in two dimensions with a fixed  $\text{TEM}_{00}$  mode laser beam focused at the bottom of the particle is shown schematically in Fig. 1. Because of the large imaginary part of the refractive index of metal, the reflectivity of the metal surface is so large that most of the light will be reflected (reflected rays not shown in Fig. 1). When the light is focused at the bottom left of the particle (top figure in Fig. 1), the optical radiation force exerted on the metal particle, indicated by the small arrows pointing to the center inside the sphere, is larger on the right than on the left side. In other words, the lateral net force is pointing toward the focus. However, when the light is focused at the upper left of the particle (bottom figure in Fig. 1), the net force is pointing away from the focus. As the nonuniformly reflected (and absorption as will be shown below) light will only provide lateral restoring force when the beam is focused below the particle center, the metal particle can only be trapped two dimensionally.<sup>29</sup>

By using the ray optics method and considering the focus below the particle center, detailed calculations of the trapping force of micron-sized metal particles have been carried out by Gu,<sup>31,32</sup> For GNAs, the refractive index is  $0.62 + 2.08i$  at 532 nm. Both reflection and absorption are strong at this wavelength and need to be taken into account. For instance, at normal incidence, 34% of the light will be absorbed and could result in a temperature change of  $200\ ^\circ\text{C}$  or more depending on the particle size and photon flux.<sup>41</sup> Therefore, both reflection and absorption are included in our calculation to improve the accuracy.

For the refracted light, only the first refraction is necessary because of the thin skin depth of the metal, which is only a few nanometers and smaller than the size of the gold nanoparticles. In the 1970s, Roosen and Imbert<sup>33</sup> introduced another method to evaluate the optical trapping force experienced by metal particles in  $\text{TEM}_{00}$  and  $\text{TEM}_{01}$  mode<sup>33</sup> beams in which the Gaussian mode profile was included for the calculation, but they did not consider the case in which the light could be focused at the bottom of the particle (Fig. 1). We base our analysis on Roosen's expressions of radiation force, including absorption, and consider that the focus of the Gaussian beam is below the center of the metal particle (Fig. 1). The radiation forces are expressed below with the parameters defined by Roosen and Imbert.<sup>33</sup>

$$F_y = \int_0^{\pi/2} d\theta \int_0^{2\pi} \frac{E^2 \rho^2 \sin \theta \cos \theta}{2\mu_0 c^2} \text{Im}[\tau(\theta)] \sin \phi d\phi,$$

$$F_x = \int_0^{\pi/2} d\theta \int_0^{2\pi} \frac{E^2 \rho^2 \sin \theta \cos \theta}{2\mu_0 c^2} \text{Im}[\tau(\theta)] \cos \phi d\phi, \quad (1)$$

where  $E$  is the electric field,

$$E^2 = E_0^2 \exp\left(\frac{-2(\rho^2 \sin^2 \theta + \rho_0^2 - 2\rho\rho_0 \sin \theta \sin \phi)}{w^2}\right) \quad (2)$$

and  $\rho$  is the radius of the metal sphere,  $\rho_0$  is the distance between the laser axis and the sphere center,  $w$  is the beam waist,  $\phi$  is the in-plane Euler angle in the local spherical coordinate system,  $\theta$  is the incident angle for a single ray, and  $\tau(\theta)$  is the transmission intensity factor depending on the ray path which is defined as

$$\tau(\theta) = 1 + R \exp(-2j\theta) - \frac{T^2 \exp(-2j\theta)}{\exp(-2j\theta_1) + R}. \quad (3)$$

The  $\text{TEM}_{00}$  mode in our system is described as a Gaussian function instead of using a plane wave approximation, since the beam waist is about  $1 \mu\text{m}$  and the trapped particles are similar in size.

For each incident angle  $\theta$ , there will be a complex refractive angle,  $\theta_1$ , because of the complex refractive index of the metal particles. The reflectivity  $R$  and transmittance  $T$  are calculated using the complex refractive index and the incident angle of each ray, respectively. Because of the strong absorption of GNAs at 532 nm, it is necessary to include the refraction and absorption. Furthermore, because of the strong absorption, it is not appropriate to only consider the trapping force; the light-induced heating must also be considered, as has been pointed out and considered by others.<sup>28–32</sup>

The light-induced heating results in the radiometric force<sup>36–38</sup> that is another important factor in the observed trapping and agglomeration. The metal nanoparticles inside the trapping beam will be heated nonuniformly due to the nonuniform intensity distribution of the Gaussian beam. The particles in the higher intensity region (near the beam center) are heated to a higher temperature, therefore they move faster, recoil back, are pushed out of the focus.<sup>36</sup> Previously, levitation by radiometric forces was observed with glycerol spheres that were impregnated with dye in the air at low pressure.<sup>36</sup> For metal particles, the absorption coefficient is large, especially for gold and silver at 532 nm, and radiometric force is thus expected to be strong.

Yalamov<sup>42</sup> has shown the expression of radiometric force  $F_r$  as

$$\vec{F}_r = -\frac{4\pi R_p \eta_e^2 J K \vec{I}}{\rho_g T_s K_i}, \quad (4)$$

where all the parameters were given in detail by Arnold.<sup>37</sup> Briefly,  $R_p$  is the radius of the particle, and  $T_s$  is the surface temperature,  $\eta_e$  is the viscosity of the water, and  $\rho_g$  is the density of metal particles.  $K_i$  is the interior thermal conductivity, which is related to the thermal property of the active material.

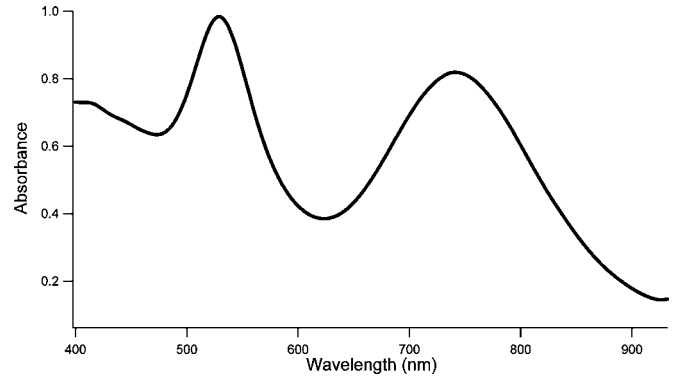


FIG. 4. UV-visible absorption spectrum of gold nanoparticle aggregate solution. Concentration was as prepared and as used in trapping experiments.

## IV. EXPERIMENTAL RESULTS

### A. UV-visible spectrum, TEM, and AFM of gold nanoparticles (aggregates)

The UV-visible electronic absorption spectrum (Fig. 4) of the GNAs shows two bands in the visible to near IR region, one peaked at 530 nm and another near 760 nm. The 530 nm band is the transverse surface plasmon absorption, typical for gold nanoparticles, while the 760 nm band has been attributed to strong interaction between nanoparticles in the aggregates, termed extended plasmon band (EPB).<sup>43</sup> The width and location of the EPB strongly depends on the size and the shape of the aggregates.

Representative TEM and AFM images of the GNAs are shown in Fig. 5. Based on the TEM and AFM data, the average size of the aggregates varies from 100 nm to over 2000 nm and each aggregate is composed of many strongly interacting gold nanoparticles with an average diameter between 5 and 10 nm.

### B. Observation of optical trapping of nanoparticles (aggregates)

Figure 6 shows a single GNA,  $2 \mu\text{m}$  in diameter, trapped stably in two dimensions. Larger cylindrical, elliptical, or spherical aggregates up to  $3 \mu\text{m}$  were also trapped with a  $\text{TEM}_{00}$  mode laser beam (532 nm) with approximately 50 mW power and a beam waist of about  $1 \mu\text{m}$ . The micron-sized metal structure could only be trapped in the periphery of the beam when focused at the bottom of the aggregate (Fig. 6).

Although our experimental setup does not allow direct observation of trapping of individual isolated gold or silver nanoparticles smaller than a few hundred nanometers since they are much smaller than the diffraction limit of the experimental system, we did observe trapping of aggregates with regular shapes and diameters about  $1\text{--}2 \mu\text{m}$  that were formed from the isolated particles. The mechanism for aggregation is believed to be largely caused by light- or heat-induced ion detachment, as discussed in Sec. III C.

### C. Observation of light-induced agglomeration

Besides the successful optical trapping of GNAs, agglomeration of the GNAs was also observed under light illumina-

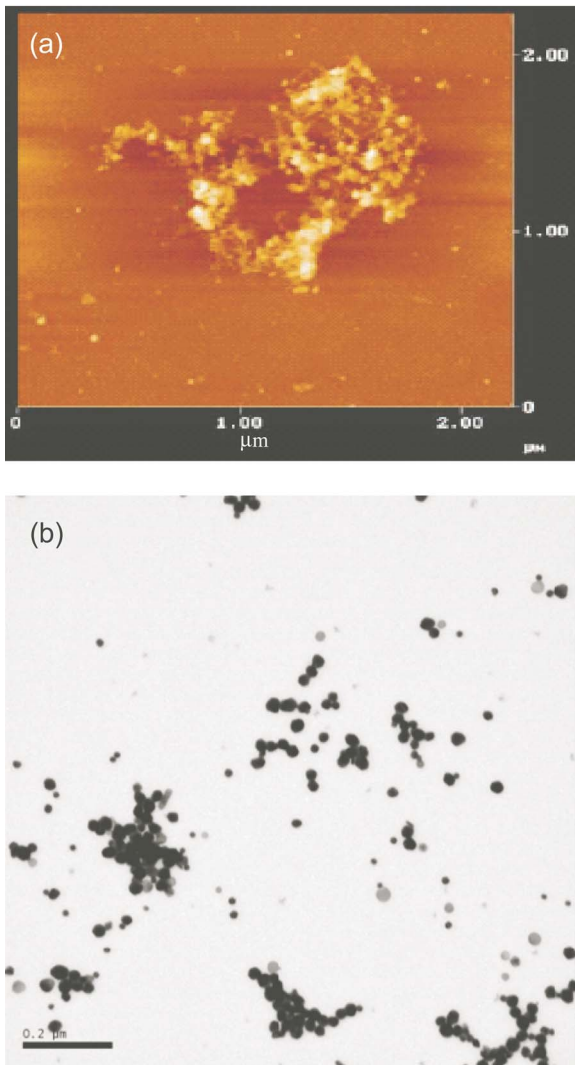


FIG. 5. (Color online) (a) AFM image showing the three-dimensional structure of the gold nanoparticle aggregates. (b) A representative TEM image of aggregates formed by gold nanoparticles (around 10 nm in diameter), with a variety of aggregate sizes and shapes.

tion. This agglomeration only took place at some particular locations, where the GNAs of about 1–2  $\mu\text{m}$  are deposited on the glass slide. The agglomeration occurred more quickly for larger sized aggregates, e.g., in the 1–2  $\mu\text{m}$  range. Figure 7 shows images of the agglomeration process. Typically, some aggregates were first attracted and trapped close to the focus region of the laser beam (as what happened in Fig. 6), since the metal particles could not be stably trapped in the focus and the particles would be pushed away to the peripheral region. Within 10 to 15 s, more aggregates were attracted to the laser beam and collected in the peripheral region of the laser beam [Fig. 7(b)]. Agglomeration began to take place when the laser beam was shifted a few micrometers to the peripheral region of the collected aggregates. We observed that the GNAs as far as 100 micrometers away were sucked into the agglomeration region and began to form a ring microstructure [Fig. 7(c)]. Eventually, on the time scale of 1–5 min, a large donut-shaped microstructure

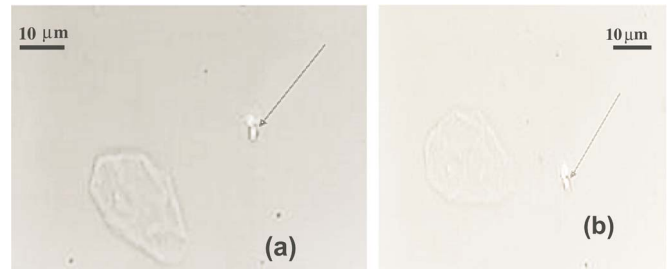


FIG. 6. (Color online) Microscopic images of a two-dimensionally trapped GNA (approximately 2  $\mu\text{m}$ ) by using a fixed Verdi laser beam of  $\text{TEM}_{00}$  mode (a) before and (b) after the movement of the glass slide. The arrow points to the darker aggregate trapped at the periphery of the beam. The bright spot is the laser focus which is not totally filtered out. The larger aggregate on the left is shown as a reference point.

with an outer diameter approximately 60  $\mu\text{m}$  was formed and the hole in the center had a diameter of about 15  $\mu\text{m}$ , and it became stabilized [Fig. 7(d)]. The bright spot in the center of the agglomerate was the focal spot of the laser beam. After the donut-shaped microstructure was fully grown and the laser beam was blocked, it would be stable for 10–20 min before it eventually broke apart or redispersed into smaller aggregates or nanoparticles again. This photoinduced agglomeration process was easily reproducible. Occasionally, the microstructure was stable for longer periods of time. If one of these stable samples was left to dry, a disk of gold nanoparticles (aggregates) with a hole in the center could be clearly observed on the glass substrate under a microscope.

To determine the effect of the laser beam shape and power on the agglomeration, two different beam patterns, circular and elliptical, with various power levels were used. An elliptical beam pattern was obtained by replacing one of the convex spherical lenses of the beam expander with a cylindrical lens. The microstructure formed became elliptical rather than circular when a cylindrical lens was used (Fig. 7). The size of this agglomerate structure as well as the rate of formation increased when the power of the laser was increased.

Possible manipulation of the agglomerate with a laser beam was also investigated. After the formation of the agglomerate, if the glass slide was moved laterally by 2–5  $\mu\text{m}$ , the metal agglomerate initially moved together with the glass slides, then jumped rapidly to the shifted new focal point, showing that it was trapped. The agglomerate did not follow if the laser beam was moved farther away (e.g.,  $\sim 20 \mu\text{m}$ ).

As mention in Sec. III B, large agglomerates can also be observed if the starting sample solution contains isolated silver or gold nanoparticles. These large agglomerates are believed to originate from smaller aggregates that were formed from isolated particles due to surface ion detachment by the laser light or heat. The experimental setup only allows us to observe the aggregates (agglomerates) when they reach a certain size (over several hundreds of nanometers).

#### D. Measurement of electrical conductivity of gold aggregates solution

It observed that when the GNAs solution was illuminated with a laser beam at 532 nm, the electrical conductivity of

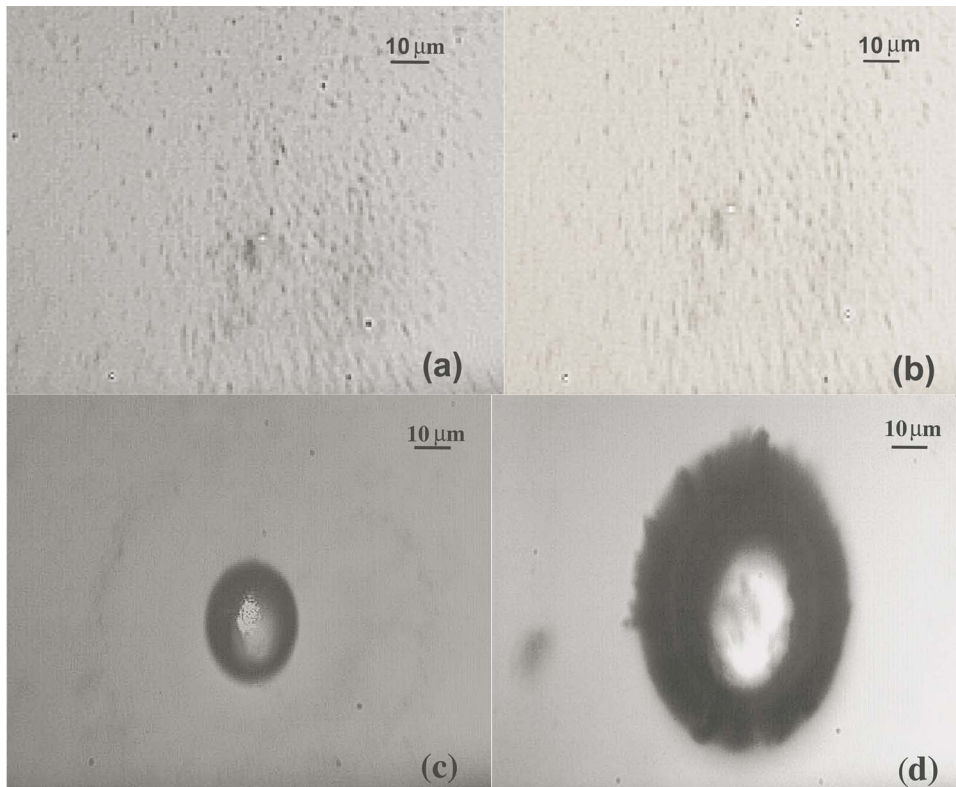


FIG. 7. (Color online) Microscopic images of the formation process of agglomeration induced by light from a Verdi laser at 50 mW. (a) Beginning of the trapping and agglomeration process, there are many aggregates (1–2 μm in size) in the center region. (b)  $t=15$  s of light illumination, more aggregates of 1–2 μm in size were attracted and deposited to the bottom of solution on the glass slide; (c)  $t=20$  s of illumination: a large agglomerate formed suddenly at the consumption of the small aggregates located within a radius of about 50 μm. The formed agglomerate then continued to grow by attracting more aggregates from the solution. (d)  $t=60$  s of illumination: final state of the agglomerate, almost all the small aggregates (1~2 μm) in the viewing area on the glass slide were attracted to and became part of the large donut-shaped agglomerate, which has an elliptical shape because a cylindrical lens was used resulting in an elliptical focus.

the solution increased quite drastically (Fig. 8). During the illumination, the temperature of the solution increased from 30 °C to 50 °C in 5 min while the electrical current increased from 15 μA to 22 μA, indicating an increase of the electrical conductivity of the solution.

To determine if the conductivity increase was due to heating as a result of laser illumination, a hot plate was utilized as a direct heat source. The current was found to increase from 15 μA to 18 μA when the solution temperature was changed from 30 °C to 50 °C (Fig. 8).

### V. SIMULATION RESULTS

Figure 9 shows the simulation results of the optical trapping force as well as the radiometric force exerted on a 1 μm gold particle by using the model introduced above. By focusing the Gaussian beam 0.5 μm below the center of the particle, it can be seen that there is an attractive force in the peripheral region of the beam, although in the center of the beam the radiation force is still repulsive. One can see that the maximum trapping force (with the radiometric force) is about 4.8 pN and it has an effective region about twice the size of the beam waist. In the center there is a 4 pN repulsive force. Only the lateral force is calculated in this two-dimensional trapping case. A 0.7 pN repulsive radiometric

(thermal) force is also added to the radiation (trapping) force. Compared with the radiation force, the radiometric force is smaller but it is not negligible and it is repulsive near the center of the laser beam.

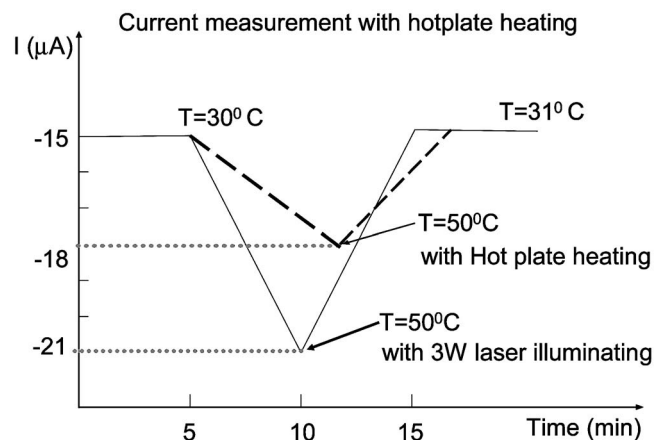


FIG. 8. Comparison of the current change of the gold nanoparticle aggregate solution due to heating by the hot plate or by laser illumination. The temperature was monitored to ensure that the temperature change was the same or very similar for the two cases.

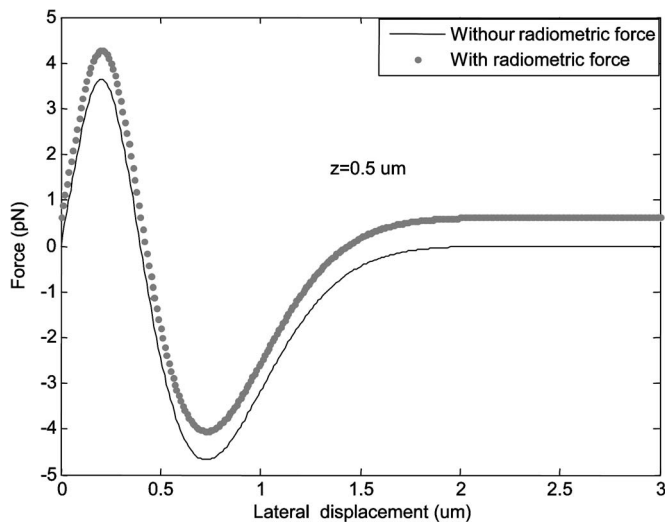


FIG. 9. Simulation results of transverse trapping forces  $F_x$  (pN) as a function of the transverse displacement for a single gold particle (radius =  $1 \mu\text{m}$ ) from the center of the focal point of the laser beam. The radiometric force is included for correction. There is a net repulsive force at the beam center when laser beam is focused  $z = 0.5 \mu\text{m}$  below the center of the particle.

## VI. DISCUSSION

### A. Mechanism of optical trapping

As mentioned earlier, two forces, radiation force and radiometric (thermal) force, are usually involved in the optical trapping of particles. For micron-sized metal particles, ray-optics approximation can be used to evaluate the radiation force and multiple internal reflections do not need to be considered because of the strong absorption of the metal. Radiometric force caused by the strong absorption of metal particles could be generated by the asymmetric heat flow. This may destabilize the trapping.

As shown by the simulation results in Fig. 9, there is a maximum of 4.8 pN attractive radiation force in the peripheral area and a 3.5 pN repulsive force in the center of the Gaussian beam (without radiometric force). The force distribution is central symmetric, which is consistent with the experimental observation of both trapping and agglomeration. The radiation force will help hold together the nanoparticles (aggregates) and possibly initiate further agglomeration.

On the other hand, the radiometric force<sup>36–38</sup> is generally repulsive, as shown in Fig. 9. As a result, particles (aggregates) will be repelled from the center of the laser focus. This explains our observation (shown in Fig. 6) that a micron-sized GNA can only be trapped at the peripheral region of the laser focus spot. In our simulation results shown in Fig. 9, the radiometric force adds to the repulsive radiation (trapping) force in the center of the beam, resulting in a hole in the central region. This is consistent with what has been predicted theoretically by Sato *et al.*<sup>29</sup> previously. To our knowledge, Sato *et al.*<sup>29</sup> is the first experimental observation to confirm this prediction.

To fully understand the details of the radiation and radiometric forces, a model that takes into account the detailed size, shape, and arrangement information of the constituent

nanoparticles, as well as the irregular shape of the aggregate, needs to be established. The results reported here provide an order of magnitude estimate and indicate that there are other factors involved in the observed agglomeration.

### B. Mechanism of agglomeration

To understand the agglomeration phenomenon observed, it is not sufficient to consider only the radiation force and the radiometric force, because the optical trapping force extends to only twice the size of the beam waist (Fig. 9). For the large agglomerates, the size is about 40–50 times larger than the beam waist ( $w = 1 \mu\text{m}$ ). Here we suggest another factor to consider, namely photothermal ion detachment from the surface of nanoparticles (aggregates).

The GNAs consists of many 5–10 nm nanoparticles as the fundamental components (Fig. 4). The surface chemistry of the Au particles is quite complex and not well understood. However, it has been suggested that the capping layer of the gold nanoparticles (aggregates) consists of negatively charged ions containing sulfur and oxygen that stabilizes the nanoparticles (aggregates).<sup>44</sup> As a result, the surface of the nanoparticles (aggregates) is negatively charged. This has been confirmed recently using gel electrophoresis measurement in our lab. The negative charges on the nanoparticles (aggregates) prevent them from forming larger aggregates or agglomerating due to repulsive forces between them. Any removal of the surface ions would destabilize the nanoparticles (aggregates) and result in agglomeration due to reduced charge screening.

Due to its strong optical absorption at the laser wavelength used and the high intensity of the focused laser beam, the nanoparticles (aggregates) quickly convert the light energy into thermal energy, initially resulting in a substantial increase in the local temperature of the particles, and eventually causing a global temperature increase of the colloidal solution.<sup>41</sup> This quick and substantial increase in temperature could liberate a significant amount of capping ions from the particle surface. We suggest that removal of surface ions, which help to stabilize the original nanoparticles and aggregates, due to laser-induced heating results in the observed light-induced agglomeration of the nanoparticles (aggregates).

If this suggestion is correct, one could expect a change in the electrical conductivity of the nanoparticles (aggregate) solution upon laser illumination due to ions released from the particle surface. To test this idea, the electrical conductivity change of the metal nanoparticles (aggregate) solution has been measured (Fig. 3 and Fig. 8). As expected, a noticeable increase in the conductivity (current) was measured upon light illumination of the nanoparticles (aggregate) solution. The temperature of the solution was monitored at the same time and found to increase with the laser illumination. The increase in global (solution) temperature alone could increase the ion mobility and hence solution conductivity. In order to decouple the effect of global heating (averaged for the entire solution sample) from that of local heating [nanoparticles (aggregates) heated by the laser light directly before equilibrating with the entire solution], a similar experiment

was performed with direct heating without light.

By heating the solution on a hot plate, we examined the effect of global heating on ion mobility in solution and possible ion liberation from the nanoparticles (aggregates), both of which can contribute toward the solution conductivity change. As shown in Fig. 8, the conductivity clearly increased with heating of the solution in the same temperature range as in the laser illumination experiment (30–50 °C). However, the increase in conductivity due to thermal heating by the hot plate is noticeably less than that due to laser illumination. The difference between the two measurements is likely due to the liberation of capping ions from the particle surface by laser-induced heating, which results in a local temperature of the particles much higher than the average temperature measured for the entire solution by a thermometer.

In the case of direct thermal heating by a hot plate, ion mobility is expected to increase with the increased temperature, which results in an increase of the conductivity or current. Liberation of capping ions from the nanoparticles (aggregate) surface is possible but not very significant within the temperature range under study.<sup>45</sup> Therefore, the increase in ion mobility is suggested as the predominant factor in the observed increase in conductivity with heating.

In the case of laser illumination, the average solution temperature increase was the same as in the thermal heating experiment. One would expect the same conductivity increase if the effect of the laser is the same as direct thermal heating. The fact that the conductivity increase is noticeably more with laser illumination than with thermal heating suggests that additional contributions must be taken into account. One possible explanation is that, besides heat generated from the laser, direct detachment or liberation of ions is induced by photoexcitation. Another possible explanation is that the local temperature of the nanoparticles (aggregates) might be much higher with the initial light absorption than the average temperature measured using a thermometer globally. A higher local temperature would also result in the release of more ions from the particle surface. The liberation from the particle surface, due to direct photoexcitation or photoinduced local heating, was consistent with the larger increase in conductivity or current in the laser illumination experiment. Very importantly, this explanation is consistent with the light-induced agglomeration observed, since ion lib-

eration from the surface of nanoparticles (aggregates) is expected to result in the formation of agglomerates.

It was noticed that the microstructured agglomerates could be redissolved or redispersed into nanoparticles (aggregates) after the laser illumination was stopped if the solution was not dried up. This observation is consistent with the suggestion of photothermal ion detachment from the metal surface. It is a dynamic process for the capping ions to leave or attach to the surface of the nanoparticles (aggregates). Upon laser illumination or direct heating, surface ions detach from the particle surface, resulting in agglomeration. When laser illumination is stopped, the ions can attach to the surface of the agglomerates and shift the equilibrium toward nanoparticles and aggregates.

## VII. CONCLUSION

The optical trapping of micron-sized metal gold nanoparticle aggregates (GNAs) with a TEM<sub>00</sub> mode laser light at 532 nm has been demonstrated. Besides the successful optical trapping of 1–3 μm GNAs, an unusual light-induced agglomeration of GNAs has also been observed. By illuminating the nanoparticles with a 50 mW focused laser beam, a 60–100 μm donut-shaped metal microstructure was formed in a GNA solution. The size of the agglomerate microstructure is proportional to the power of the laser. This agglomeration phenomenon, along with optical trapping of the nanoparticles (aggregates), was analyzed by considering radiation force, radiometric force, together with surface ion detachment caused by laser-induced heating. The observed electrical conductivity changes of the nanoparticles (aggregate) solution upon light illumination supports the suggestion of photothermal ion detachment. The results indicate the possibility of using light to control the surface properties of nanomaterials and thereby to design and fabricate microstructures from nanomaterials for device applications in nanotechnology.

## ACKNOWLEDGMENTS

This research is supported by the National Science Foundation (Grants No. ECS-0401206 and CHE-0456130) and by University of California at Santa Cruz, Special Research Grants.

\*Electronic address: [claire@soe.ucsc.edu](mailto:claire@soe.ucsc.edu)

†Electronic address: [zhang@chemistry.ucsc.edu](mailto:zhang@chemistry.ucsc.edu)

<sup>1</sup>P. B. Johnson and R. W. Christy, *Phys. Rev. B* **6**, 4370 (1972).

<sup>2</sup>M. Kerker, *J. Colloid Interface Sci.* **105**, 297 (1985).

<sup>3</sup>M. Quinten, *Z. Phys. B: Condens. Matter* **101**, 211 (1996).

<sup>4</sup>K. L. Kelly, E. Coronado, L. Zhao, and G. C. Schatz, *J. Phys. Chem. B* **107**, 668 (2003).

<sup>5</sup>A. M. Schwartzberg, C. D. Grant, A. Wolcott, C. Talley, T. Huser, R. Bogomolni, and J. Z. Zhang, *J. Phys. Chem. B* **108**, 19191 (2004).

<sup>6</sup>T. J. Norman, Jr., C. D. Grant, Donny Magana, J. Z. Zhang, J.

Liu, D. Cao, and F. B. Anthony Van, *J. Phys. Chem. B* **106**, 7005 (2002).

<sup>7</sup>J. M. Gerardy and M. Ausloos, *Phys. Rev. B* **25**, 4204 (1982).

<sup>8</sup>M. P. J. van Staveren, H. B. Brom, and L. J. de Jongh, *Solid State Commun.* **60**, 19 (1986).

<sup>9</sup>J. J. Mock, B. D. R. Smith, D. A. Schultz, and S. Scheltz, *J. Chem. Phys.* **116**, 6755 (2002).

<sup>10</sup>M. Moskovits, *Rev. Mod. Phys.* **57**, 783 (1985).

<sup>11</sup>K. Kneipp, H. Kneipp, I. Itzkan, R. R. Dasari, and M. S. Feld, *J. Phys.: Condens. Matter* **14**, 597 (2002).

<sup>12</sup>P. Kambhampati, C. M. Child, M. C. Foster, and A. Campion, *J.*

- Chem. Phys. **108**, 5013 (1998).
- <sup>13</sup>K. Kneipp, H. Kneipp, I. Itzkan, R. R. Dasari, and M. S. Feld, Chem. Rev. (Washington, D.C.) **99**, 2957 (1999).
- <sup>14</sup>A. Campion and P. Kambhampati, Chem. Soc. Rev. **27**, 241 (1998).
- <sup>15</sup>A. Otto, Phys. Status Solidi A **188**, 1455 (2001).
- <sup>16</sup>B. J. Messinger, K. U. von Raben, R. K. Chang, P. W. Barber, Phys. Rev. B **24**, 649 (1981).
- <sup>17</sup>F. J. Garcia-Vidal and J. B. Pendry, Phys. Rev. Lett. **77**, 1163 (1996).
- <sup>18</sup>M. Quinten, J. Cluster Sci. **10**, 319 (1999).
- <sup>19</sup>M. Quinten, Appl. Phys. B: Lasers Opt. **73**, 245 (2001).
- <sup>20</sup>A. Michaels, M. Jiang, and L. Brus, J. Phys. Chem. B **104**, 11965 (2000).
- <sup>21</sup>A. N. Shipway, M. Lahav, R. Gabai, and I. Willner, Langmuir **16**, 8789 (2000).
- <sup>22</sup>M. Quinten and U. Kreibig, Appl. Opt. **32**, 6173 (1993).
- <sup>23</sup>S. Nahal, H. R. M. Kholesifard, and J. Mostafavi-amjadi, Appl. Phys. B: Lasers Opt. **79**, 513 (2004).
- <sup>24</sup>A. Ashkin, Biophys. J. **61**, 569 (1992).
- <sup>25</sup>A. Ashkin, IEEE J. Sel. Top. Quantum Electron. **6**, 841 (2000).
- <sup>26</sup>P. Jordan, J. Cooper, G. McNay, F. T. Docherty, D. Graham, W. E. Smith, G. Sinclair, and M. J. Padgett, Opt. Express **13**, 4148 (2005).
- <sup>27</sup>H. Furukawa and I. Yamaguchi, Opt. Lett. **23**, 216 (1998).
- <sup>28</sup>K. Svoboda and S. M. Block, Opt. Lett. **19**, 930 (1994).
- <sup>29</sup>S. Sato, Y. Harada, and Y. Waseda, Opt. Lett. **19**, 1807 (1994).
- <sup>30</sup>H. Rubinsztein-Dunlop, T. A. Nieminen, M. E. J. Friese, and N. R. Heckenberg, Adv. Quantum Chem. **30**, 469 (1998).
- <sup>31</sup>M. Gu and D. Morrish, J. Appl. Phys. **91**, 1606 (2002).
- <sup>32</sup>P. C. Ke and M. Gu, Appl. Opt. **38**, 160 (1999).
- <sup>33</sup>G. Roosen and C. Imbert, Opt. Commun. **26**, 432 (1978).
- <sup>34</sup>J. P. Barton, D. R. Alexander, and S. A. Schaub, J. Appl. Phys. **66**, 4594 (1989).
- <sup>35</sup>J. P. Barton and D. R. Alexander, J. Appl. Phys. **66**, 2800 (1989).
- <sup>36</sup>M. Lewittes, S. Arnold, and G. Oster, Appl. Phys. Lett. **40**, 455 (1982).
- <sup>37</sup>S. Arnold, A. B. Pluchino, and K. M. Leung, Phys. Rev. A **29**, 654 (1984).
- <sup>38</sup>S. Arnold and M. Lewittes, J. Appl. Phys. **53**, 5314 (1982).
- <sup>39</sup>J. Turkevich, P. L. Stevenson, and J. Hillier, Trans. Faraday Soc. **55**, 234 (1951).
- <sup>40</sup>P. C. Lee and D. Meisel, J. Phys. Chem. **86**, 3391 (1982).
- <sup>41</sup>M. Hu and G. V. Hartland, J. Phys. Chem. B **106**, 7029 (2002).
- <sup>42</sup>Y. I. Yalamov, V. B. Kutukov, and E. R. Suchukin, J. Colloid Interface Sci. **57**, 56 (1976).
- <sup>43</sup>C. D. Grant, A. Schwartzberg, T. Norman, Jr., and J. Z. Zhang, J. Am. Chem. Soc. **125**, 549 (2003).
- <sup>44</sup>T. Norman, Jr., C. Grant, D. Magana, R. Anderson, J. Z. Zhang, D. Cao, F. Bridges, J. Liu, and T. van Buuren, Proc. SPIE **4807**, 51 (2002).
- <sup>45</sup>L. Vlaev and V. Georgieva, J. Solution Chem. **34**, 961 (2005).